

Article

Comparison of Different Metal Doping Effects on Co_3O_4 Catalysts for the Total Oxidation of Toluene and Propane

Weidong Zhang ¹, Paola Anguita ¹, Javier Díez-Ramírez ², Claude Descorme ¹ ,
Jose Luis Valverde ²  and Anne Giroir-Fendler ^{1,*}

¹ Univ. Lyon, Université Claude Bernard Lyon 1, CNRS, IRCÉLYON, 2 Avenue Albert Einstein, 69622 Villeurbanne, France; weidong.zhang@ircelyon.univ-lyon1.fr (W.Z.); Paola.anguita@gmail.com (P.A.); claude.descorme@ircelyon.univ-lyon1.fr (C.D.)

² Department of Chemical Engineering, Faculty of Chemical Science and Technology, University of Castilla-La Mancha, Avenida Camilo José Cela 12, 13005 Ciudad Real, Spain; javier.diez@uclm.es (J.D.-R.); jlvalverde1964@gmail.com (J.L.V.)

* Correspondence: anne.giroir-fendler@ircelyon.univ-lyon1.fr; Tel.: +33-472-431-586

Received: 9 July 2020; Accepted: 27 July 2020; Published: 3 August 2020



Abstract: Metal-doped (Mn, Cu, Ni, and Fe) cobalt oxides were prepared by a coprecipitation method and were used as catalysts for the total oxidation of toluene and propane. The metal-doped catalysts displayed the same cubic spinel Co_3O_4 structure as the pure cobalt oxide did; the variation of cell parameter demonstrated the incorporation of dopants into the cobalt oxide lattice. FTIR spectra revealed the segregation of manganese oxide and iron oxide. The addition of dopant greatly influenced the crystallite size, strain, specific surface area, reducibility, and subsequently the catalytic performance of cobalt oxides. The catalytic activity of new materials was closely related to the nature of the dopant and the type of hydrocarbons. The doping of Mn, Ni, and Cu favored the combustion of toluene, with the Mn-doped one being the most active ($14.6 \times 10^{-8} \text{ mol g}_{\text{Co}}^{-1} \text{ s}^{-1}$ at $210 \text{ }^\circ\text{C}$; $T_{50} = 224 \text{ }^\circ\text{C}$), while the presence of Fe in Co_3O_4 inhibited its toluene activity. Regarding the combustion of propane, the introduction of Cu, Ni, and Fe had a negative effect on propane oxidation, while the presence of Mn in Co_3O_4 maintained its propane activity ($6.1 \times 10^{-8} \text{ mol g}_{\text{Co}}^{-1} \text{ s}^{-1}$ at $160 \text{ }^\circ\text{C}$; $T_{50} = 201 \text{ }^\circ\text{C}$). The excellent performance of Mn-doped Co_3O_4 could be attributed to the small grain size, high degree of strain, high surface area, and strong interaction between Mn and Co. Moreover, the presence of 4.4 vol.% H_2O badly suppressed the activity of metal-doped catalysts for propane oxidation, among them, Fe-doped Co_3O_4 showed the best durability for wet propane combustion.

Keywords: metal doping; cobalt oxide; synergistic effect; VOC oxidation; toluene; propane

1. Introduction

Hydrocarbons emitted from both industrial manufacture and motor vehicle exhaust cause a lot of atmospheric pollution. Catalytic combustion is one of the most promising countermeasures for the elimination of hydrocarbons. As an inexpensive and active catalyst, Co_3O_4 has attracted much interest in the past decade as a substitute for the noble metal catalysts.

Liu et al. prepared nanocrystalline cobalt oxide by a soft reactive grinding procedure, the catalyst shows high specific rate for propane total oxidation benefiting from a high concentration of superficial electrophilic oxygen (O^-) species [1]. Garcia et al. synthesized ordered Co_3O_4 via a nanocasting method using KIT-6 as the hard template. The good activity of these catalysts in the total oxidation of toluene and propane was correlated with both the high surface area and the presence of oxygen vacancies instead of the ordered structure [2]. Marin et al. produced very active Co_3O_4 catalyst with

50% propane conversion at 175 °C using a supercritical CO₂ anti-solvent precipitation method [3]. Salek et al. obtained Co₃O₄ with high porosity by moderate calcination of CoO(OH) derived from aqueous precipitation. This catalyst showed a superior activity for CO and propane total oxidation [4]. By using an acetic acid leaching strategy, Tang and his co-workers modified the surface structure and chemistry of Co₃O₄ nanoparticles and obtained a Co₃O₄ catalyst with more abundant defects, surface Co²⁺, and chemisorbed oxygen species, which presented a much higher activity than the commercial Pt/Al₂O₃ and Pd/Al₂O₃ catalysts [5]. Analogously, Li et al. fabricated mesoporous Co₃O₄ via nitric acid treatment, and the as-prepared catalyst showed enhanced activity in toluene oxidation due to higher specific surface areas, more weak acidic sites, and a greater amount of surface Co²⁺ and adsorbed oxygen species [6]. Ren et al. constructed various 3D hierarchical Co₃O₄ nanocatalysts via a hydrothermal process and demonstrated that the hierarchical cube-stacked Co₃O₄ microspheres exhibited best activity for toluene oxidation [7].

Nevertheless, it is still a challenge to increase the catalytic activity of Co₃O₄ for different VOCs to broaden the feasible range and meet the need of realistic application.

Substituting a small fraction of cobalt in a Co₃O₄ lattice with another metal cation, known as doping, is a potential way to improve the performance of Co₃O₄ catalysts. The chemical bonding at the surface of Co₃O₄ could be modified by metal doping, which may in turn induce lattice imperfection and create oxygen vacancies that are beneficial to catalytic reaction. The effect of metal dopant features, including oxidation state, ionic radius, electronegativity, etc., on the physicochemical properties and redox ability of cobalt-based catalysts was extensively studied theoretically and practically [8–10].

Ni doping into a Co₃O₄ lattice enhanced propane oxidation reaction kinetics by promoting surface lattice oxygen activity and facilitating CO₂ desorption [11]. The incorporation of Mn in Co₃O₄ increased surface Co²⁺ concentration and active oxygen, contributing to high activity in catalytic combustion of 1,2-dichlorobenzene (o-DCB) and retarding chlorination of o-DCB [12]. The doping of In₂O₃ induced the structural distortion of Co₃O₄ and promoted the catalytic performance of Co₃O₄ for CO oxidation [13]. Baidya et al. demonstrated that 15% Fe-doped Co₃O₄ can achieve superior catalytic activity and stability towards CO oxidation [14].

Although there have already been some reports on metal-doped Co₃O₄ catalysts that present desirable activity, the comparative study of different metal dopant effects on the catalytic activity of Co₃O₄ in different hydrocarbons oxidation is still limited and needs to be further explored.

Recently, we have found that the precipitation agent could affect the catalytic activity of Co₃O₄. Among the investigated precipitation agent, sodium carbonate proved to be the most promising one. Considering this fact, in this study, the effect of metal-doping based on carbonate precipitation method on the physicochemical properties and redox ability of Co₃O₄ was investigated.

Herein, we prepared four metal-doped (Mn, Cu, Ni, and Fe) Co₃O₄ by a coprecipitation method. A comparative study of the catalytic behavior of pure and metal ion-substituted Co₃O₄ was investigated for the total oxidation of toluene and propane. A small amount of metal incorporated into the Co₃O₄ lattice affected the structure and redox property of Co₃O₄ and in turn led to different catalytic behavior as a function of the reactant used.

2. Results and Discussion

2.1. Chemical Composition, Structure, and Textural Properties

The chemical compositions of the as-prepared samples were determined by inductively coupled plasma optical emission spectroscopy (ICP-OES) measurement. The results are listed in Table 1. The cobalt mass ratio of pure cobalt oxide was 74.7 wt.%, close to the stoichiometric value of Co₃O₄ (73.4 wt.%). The substituted metal to cobalt molar ratios were similar to the theoretical one (5%), indicating the success of the coprecipitation process.

Table 1. Chemical composition, structural, and textural properties of the Co_3O_4 and $\text{M}_{0.05}\text{Co}$ catalysts.

Catalysts	Co (wt.%)	M/Co (at.%)	D (nm) ^a	Strain (%) ^a	a (Å) ^a	SSA ($\text{m}^2 \text{g}^{-1}$) ^b	V_{pore} ($\text{cm}^3 \text{g}^{-1}$) ^b
Co_3O_4	74.7	-	29.4	0.34	8.084	30	0.08
$\text{Mn}_{0.05}\text{Co}$	68.1	4.5	19.1	0.53	8.098	47	0.19
$\text{Cu}_{0.05}\text{Co}$	68.3	5.6	26.6	0.38	8.093	29	0.07
$\text{Ni}_{0.05}\text{Co}$	67.6	5.3	22.5	0.45	8.096	35	0.11
$\text{Fe}_{0.05}\text{Co}$	68.0	5.9	27.1	0.37	8.094	34	0.09

^a Average crystalline size (D), strain, and lattice constant (a) obtained from XRD analysis. ^b Specific surface area (SSA) and total pore volume (V_{pore}) calculated from N_2 adsorption-desorption isotherm.

Powder X-ray diffraction (XRD) patterns of pure cobalt oxide and metal-doped cobalt oxides are shown in Figure 1. It is observed that all metal-doped cobalt oxides exhibited characteristic diffraction peaks corresponding to Co_3O_4 spinel structures (lattice constant $a = 8.0840 \text{ \AA}$, PDF # 74-2120) identical to pure cobalt oxide, no matter what kind of substituted metal was used, indicating that the doped metals were uniformly distributed in the samples, either in the lattice or on the surface. However, looking at the enlarged patterns for all $\text{M-Co}_3\text{O}_4$ samples, an evident shift of the most intense peak (311) to lower angles could be seen, suggesting an increase in the lattice constant due to metal substitution. The average crystalline sizes, strains, and the lattice constants of all samples were calculated and are listed in Table 1. Compared to pure Co_3O_4 , all $\text{M-Co}_3\text{O}_4$ samples presented a smaller crystalline size, a bigger strain, and a larger lattice constant, especially for the $\text{Mn}_{0.05}\text{Co}$ sample. This result demonstrates that some M ions were successfully introduced into the crystal lattice of Co_3O_4 , leading to a lattice expansion of the spinel, thus generating a smaller crystalline size.

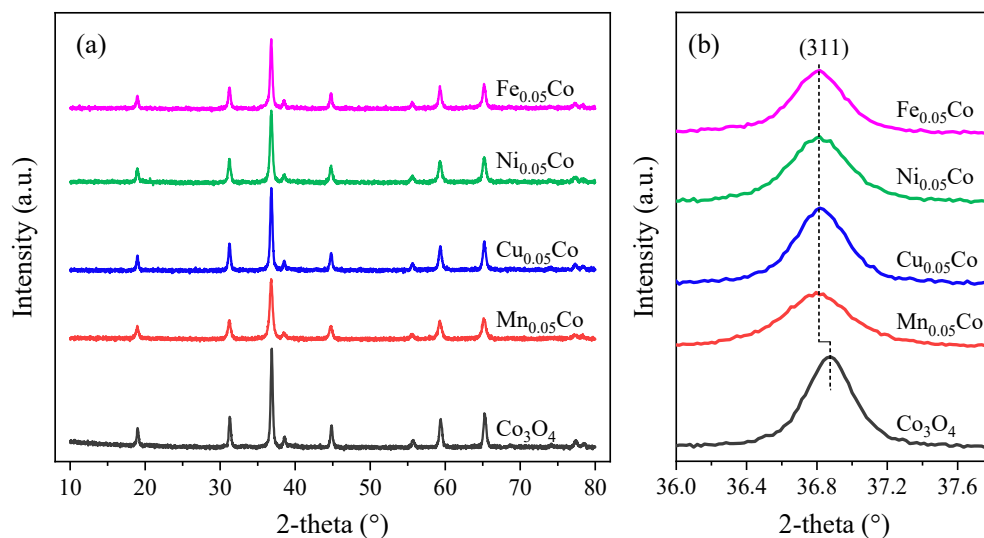
**Figure 1.** (a,b) XRD patterns of the Co_3O_4 and $\text{M}_{0.05}\text{Co}$ catalysts.

Figure 2 shows the Fourier transform infrared (FTIR) spectra of Co_3O_4 and $\text{M}_{0.05}\text{Co}$ samples. Two characteristic peaks at ca. 655 and 550 cm^{-1} (with shoulders at higher frequencies), corresponding to vibrations of Co^{3+} in tetrahedral sites and Co^{2+} in octahedral sites in Co_3O_4 spinel structure respectively [15], were observed for all samples, in agreement of XRD analysis. However, some new peaks appeared in the case of $\text{Mn}_{0.05}\text{Co}$ and $\text{Fe}_{0.05}\text{Co}$, which could be assigned to vibration modes of Mn-O and Fe-O , respectively [16,17]. In addition, the presence of Ni-O or Cu-O vibration modes could not be excluded since they were expected to be located in the same region of Co-O vibration modes and could be overlapped [18,19]. This phenomenon revealed that not all metal ions were successfully inserted into the matrix of Co_3O_4 lattice, some of them might form amorphous MO_x species and distribute on the surface.

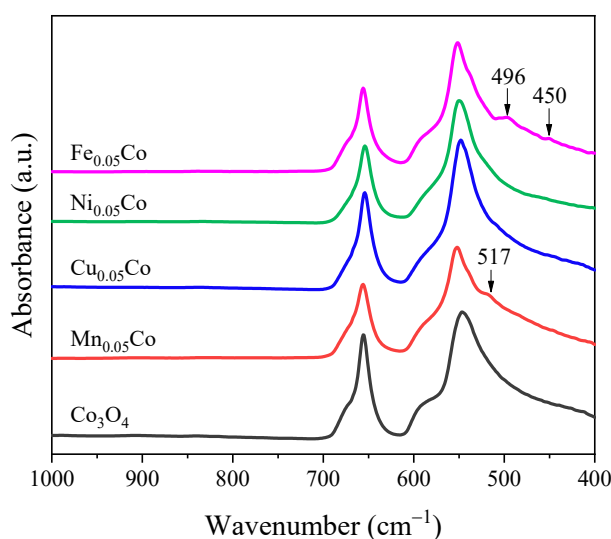


Figure 2. FTIR spectra of the Co_3O_4 and $\text{M}_{0.05}\text{Co}$ catalysts.

The N_2 adsorption–desorption isotherms and Barrett–Joyner–Halenda (BJH) pore size distributions of undoped and doped Co_3O_4 samples are displayed in Figure 3. The type IV isotherm curves and H1-shaped hysteresis loops indicated the presence of slit-type mesopores originated from the accumulation of nanoparticles. The textural parameters of the different samples are summarized in Table 1. The specific surface areas (SSA) of all samples sit in the range of 30 to $47 \text{ m}^2 \text{ g}^{-1}$. Among all samples, $\text{Mn}_{0.05}\text{Co}$ showed the largest SSA ($47 \text{ m}^2 \text{ g}^{-1}$) and biggest pore volume ($0.19 \text{ cm}^3 \text{ g}^{-1}$), followed by the $\text{Ni}_{0.05}\text{Co}$ and $\text{Fe}_{0.05}\text{Co}$ samples. It should be noted that the average crystallite size of $\text{Cu}_{0.05}\text{Co}$ was smaller than that of pure Co_3O_4 , while the SSA for $\text{Cu}_{0.05}\text{Co}$ was lower than that for pure Co_3O_4 , indicating a strong agglomeration of the crystallites.

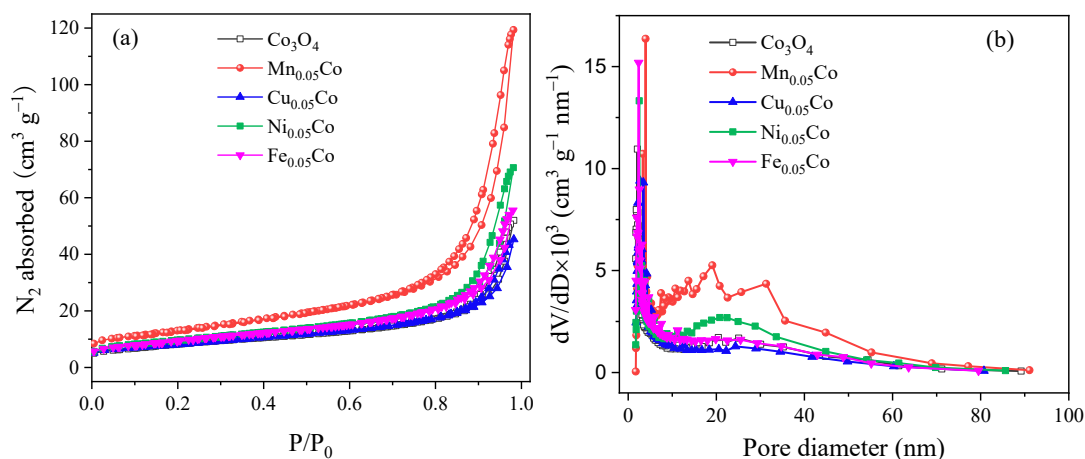


Figure 3. (a) N_2 adsorption–desorption isotherms and (b) BJH pore size distribution curves of the Co_3O_4 and $\text{M}_{0.05}\text{Co}$ catalysts.

Raman spectra were recorded to investigate the effect of metal doping on the lattice distortion of the spinel. As shown in Figure 4, five characteristic bands at 665, 601, 507, 463, and 187 cm^{-1} corresponding to stretching mode of spinel Co_3O_4 (A_{1g} , F_{2g}^3 , F_{2g}^2 , E_g , and F_{2g}^1 symmetry) were clearly observed for pure Co_3O_4 [5,20]. Compared to pure Co_3O_4 , the Raman bands of the $\text{M}_{0.05}\text{Co}$ samples weakened and broadened because of the dissolution of M into the Co_3O_4 lattice, which induced lattice expansion and lattice distortion, as revealed by XRD analysis. The peak position and full width at half maxima (FWHM) of the most intense peak are listed in Table 2. Raman spectrum of $\text{Ni}_{0.05}\text{Co}$

underwent a red-shift, while that of $\text{Fe}_{0.05}\text{Co}$ underwent a blue-shift. $\text{Ni}_{0.05}\text{Co}$ exhibited the largest FMWH while $\text{Fe}_{0.05}\text{Co}$ exhibited the smallest one.

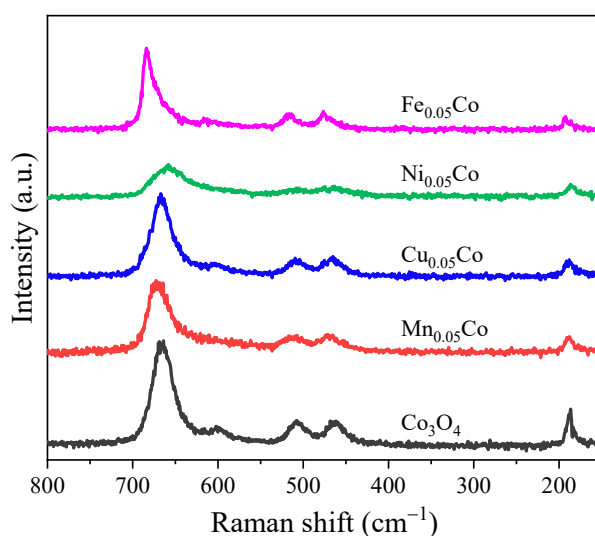


Figure 4. Raman spectra of the Co_3O_4 and $\text{M}_{0.05}\text{Co}$ catalysts.

Table 2. Raman and temperature-programmed reduction in hydrogen (H_2 -TPR) analysis of the Co_3O_4 and $\text{M}_{0.05}\text{Co}$ catalysts.

Catalysts	Raman Peak ^a (cm^{-1})	FWMH ^a	Total H_2 Uptake (mmol g^{-1})	H_2 Uptake Below 300 °C (mmol g^{-1})
Co_3O_4	667	34	16.0	3.0
$\text{Mn}_{0.05}\text{Co}$	672	37	15.0	2.5
$\text{Cu}_{0.05}\text{Co}$	667	34	13.7	8.1
$\text{Ni}_{0.05}\text{Co}$	660	46	15.0	3.2
$\text{Fe}_{0.05}\text{Co}$	684	24	13.8	2.1

^a Peak position and FWMH of the most intense Raman peak.

2.2. Reducibility

To investigate the effect of metal doping on the reducibility of Co_3O_4 , H_2 -TPR experiments were carried out; the results are shown in Figure 5, whereas the quantitative results of hydrogen consumption are summarized in Table 2. For pure Co_3O_4 , the reduction initiated at 195 °C and finished at 400 °C. Two sequent peaks corresponding to the reduction of $\text{Co}^{3+} \rightarrow \text{Co}^{2+}$ and $\text{Co}^{2+} \rightarrow \text{Co}^0$ were clearly observed at 291 and 383 °C, respectively. However, after metal doping, the positions of these two peaks clearly changed. Moreover, some small peak shoulders that may arise from the reduction of doping species appeared (indicated by the arrows). In the case of $\text{Cu}_{0.05}\text{Co}$ and $\text{Ni}_{0.05}\text{Co}$, both peaks shifted towards low temperature range, especially for $\text{Cu}_{0.05}\text{Co}$. The reduction of the Cu-doped sample started from 170 °C and ended at 360 °C, suggesting that the presence of Cu or Ni facilitated the Co_3O_4 reduction. Regarding $\text{Mn}_{0.05}\text{Co}$ and $\text{Fe}_{0.05}\text{Co}$, the low-temperature peak appeared to be similar to that of the pure Co_3O_4 , while the high-temperature peak moved to higher temperature zone, indicating that Mn or Fe doping could hinder the formation of metallic cobalt, which is beneficial for the redox circle during reaction between Co^{3+} and Co^{2+} [21]. The total hydrogen consumption amount decreased for all the metal-doped samples, suggesting the nonstoichiometric nature of the samples with metal doping. By comparing the hydrogen uptake below 300 °C, one can conclude that the low temperature reducibility ranks in the sequence $\text{Cu}_{0.05}\text{Co} > \text{Ni}_{0.05}\text{Co} > \text{Co}_3\text{O}_4 > \text{Mn}_{0.05}\text{Co} > \text{Fe}_{0.05}\text{Co}$. Based on the above reduction behaviors, Cu or Ni doping enhanced the reducibility of Co_3O_4 , whereas Mn or Fe doping worsened it. This way, $\text{Cu}_{0.05}\text{Co}$ was the most reducible sample.

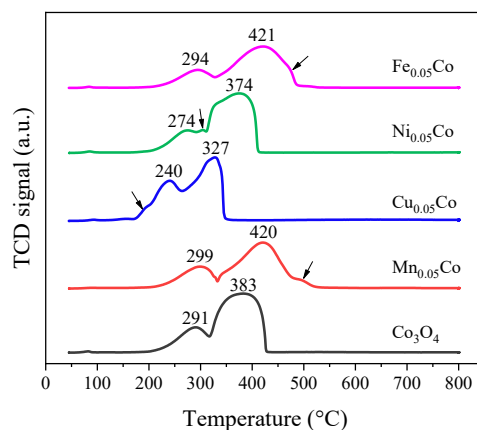


Figure 5. H₂-TPR profiles of the Co₃O₄ and M_{0.05}Co catalysts.

2.3. Catalytic Performance

2.3.1. Catalytic Activity and Stability in Toluene Oxidation

The catalytic performance of all the samples was evaluated in both toluene and propane oxidation. Regarding the toluene oxidation, three continuous heating–cooling loop tests were performed. Figure S1a presented the light-off curves of pure Co₃O₄ and metal-doped Co₃O₄ catalysts during the third continuous heating run. In the high conversion stage, toluene conversion to CO₂ exceeds 100% due to the accumulation of intermediates during the low conversion period [22]. Considering this fact, the light-off curves during the third continuous cooling run were used and are displayed in Figure 6, whereas the light-off temperatures at 10, 50, and 90% toluene conversion (T₁₀, T₅₀, and T₉₀) were listed in Table 3. The difference among the three catalytic cycles was imperceptible, demonstrating the excellent cycle stability of the Co₃O₄ and M_{0.05}Co catalysts. All catalysts were able to achieve full conversion of toluene to CO₂ below 280 °C. After doping with Mn, Cu, or Ni, the catalytic performance of pure Co₃O₄ was obviously improved, being that the light-off curve shifted to lower temperature. However, the incorporation of Fe into Co₃O₄ resulted in a worse performance. Notably, the catalytic performance enhancement by metal doping is more pronounced in the low temperature stage than in the high one. In addition, the concentrations of CO produced during the toluene oxidation process over all catalysts were below 110 ppm (Figure S2a). Among them, Fe_{0.05}Co with poor catalytic efficiency showed inferior selectivity. Nevertheless, the calculated carbon balances at 300 °C for all catalysts were higher than 95%, indicating the decent selectivity of the as-prepared cobalt-based catalysts.

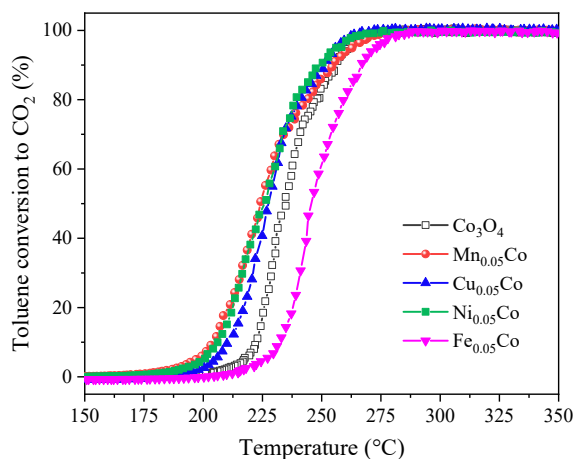


Figure 6. Variation of the toluene conversion with the reaction temperature during the third consecutive cooling run over the Co₃O₄ and M_{0.05}Co catalysts.

Table 3. Light-off temperatures at 10, 50, and 90% toluene conversion upon the cooling process.

Catalysts	1st Run			2nd Run			3rd Run		
	T ₁₀	T ₅₀	T ₉₀	T ₁₀	T ₅₀	T ₉₀	T ₁₀	T ₅₀	T ₉₀
Co ₃ O ₄	223	235	256	223	235	256	223	235	256
Mn _{0.05} Co	203	224	254	204	224	255	204	224	255
Cu _{0.05} Co	211	228	251	211	228	251	211	228	251
Ni _{0.05} Co	206	226	250	206	226	250	206	226	250
Fe _{0.05} Co	234	244	270	234	244	270	234	245	270

In order to better compare the activity, the catalytic reaction rates of all catalysts at 210 °C were calculated and are listed in Table 4. This activity ranked as follows, Mn_{0.05}Co > Ni_{0.05}Co > Cu_{0.05}Co > Co₃O₄ > Fe_{0.05}Co. Moreover, the activation energies (E_a) and pre-exponential factors (A) were estimated based on the slopes and intercepts of the Arrhenius plots (Figure S3a). Diverse values of the activation energy ranging from 142 kJ mol⁻¹ to 231 kJ mol⁻¹ were obtained. The activation energies and pre-exponential factors here showed did not correlated with the activity, which can be explained by the compensation effect (Figure S4) [23,24].

Table 4. Reaction rates (r) at 210 °C, apparent pre-exponential factors (A), apparent activation energies (E_a), and coefficient of determination (R^2) for toluene oxidation over various catalysts (reaction conditions: toluene concentration = 1000 ppm, O₂ concentration = 21 vol.%, and WHSV = 40,000 mL h⁻¹ g⁻¹).

Catalysts	r (10 ⁻⁸ mol g _{Co} ⁻¹ s ⁻¹)	lnA	E_a (kJ mol ⁻¹)	R^2
Co ₃ O ₄	1.5	30.5 ± 0.8	196 ± 3	0.995
Mn _{0.05} Co	14.6	18.7 ± 0.5	142 ± 2	0.998
Cu _{0.05} Co	6.4	40.6 ± 1.2	231 ± 5	0.997
Ni _{0.05} Co	10.2	24.3 ± 1.2	165 ± 5	0.993
Fe _{0.05} Co	0.5	35.8 ± 0.9	222 ± 4	0.997

The long-term stability of the catalysts was assessed at 20–25% of toluene conversion after the first cooling run. As shown in Figure 7, the conversion declined for all catalysts to some extent after 5 h, remaining invariable throughout the test. The Mn_{0.05}Co, Cu_{0.05}Co, and Ni_{0.05}Co catalysts exhibited similar stability, with ~15% decrease in toluene conversion during the whole process. The Co₃O₄ and Fe_{0.05}Co catalysts deactivated more severely, ~20% of toluene conversion drop was observed. In order to figure out the reason causing catalyst deactivation, a post-calcination treatment in air flow was carried out after 24 h stability test; the CO₂ evolution as a function of time on stream was plotted in Figure S5. The maximum in the CO₂ concentration could arise from the catalytic oxidation of adsorbed toluene or intermediate into CO₂ [25]. The time for reaching this maximum CO₂ concentration was dependent on the catalytic activity of the different catalysts and likely on the reaction temperatures (varied from 215 to 240 °C). The higher the reaction temperature, the faster the CO₂ desorption on the catalyst surface. The area of this peak reflected the amount of toluene/intermediate adsorbed in the catalyst. Among these catalysts, Fe_{0.05}Co exhibited the largest peak area, suggesting its excellent CO₂ adsorption capacity. To verify the reversibility of this deactivation for catalyst Co₃O₄, a stability test was conducted after the calcination treatment (Figure S6). Identical stability curve was observed after the calcination step, demonstrating that it is possible to completely regenerate the catalyst.

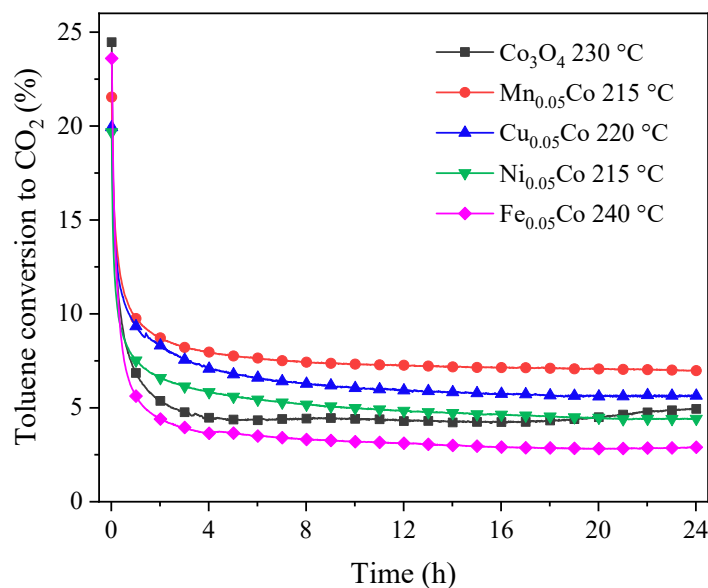


Figure 7. Toluene oxidation test conducted at 20–25% of toluene conversion during 24 h.

2.3.2. Catalytic Activity and Water Resistance in Propane Oxidation

On the other hand, the light-off curves of the propane oxidation for pure Co₃O₄ and metal-doped Co₃O₄ catalysts during the cooling run are displayed in Figure 8. Table 5 summarized the temperatures at which 10, 50, and 90% of propane conversion was reached. Propane can be converted into CO₂ below 280 °C for all of the catalysts. However, totally different trends in the catalytic performance of propane and toluene oxidation were observed. For propane oxidation, pristine Co₃O₄ was the most active catalyst. The doping with Cu, Ni, or Fe was detrimental for the catalytic performance of pure Co₃O₄, being that the light-off curve shifted to higher temperature. This detrimental phenomenon was especially remarkable over Cu_{0.05}Co. Fortunately, the catalytic performance remained practically unaltered after the incorporation of Mn. The concentrations of CO and propene produced during the propane oxidation process over all catalysts were 0 ppm (no shown) and <5 ppm (Figure S2b), respectively, suggesting the excellent selectivity of the catalysts, which was further confirmed by the good carbon balance throughout the catalytic system (>99%).

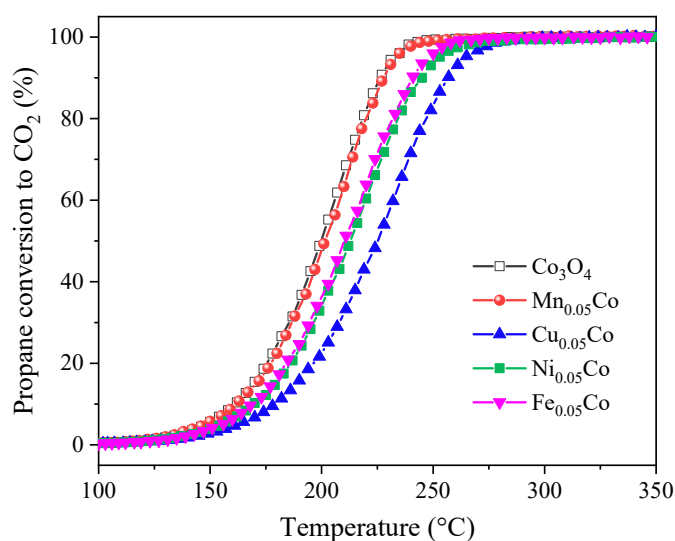


Figure 8. Variation of the propane conversion with the reaction temperature during the cooling run over the Co₃O₄ and Mn_{0.05}Co catalysts.

Table 5. Light-off temperatures at 10, 50, and 90% propane conversion upon cooling process in normal condition or in the presence of 4.4 vol.% water.

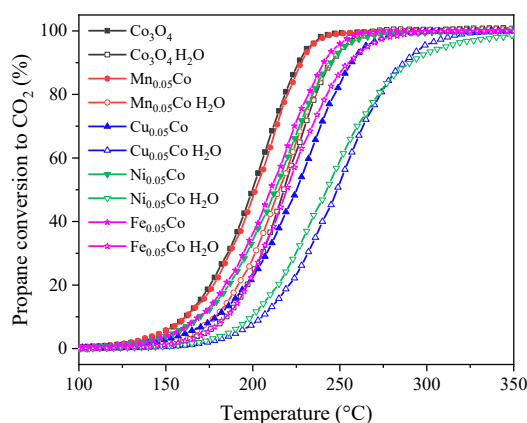
Catalysts	Normal Condition			In 4.4 vol.% Water		
	T ₁₀	T ₅₀	T ₉₀	T ₁₀	T ₅₀	T ₉₀
Co ₃ O ₄	161	199	226	185	218	245
Mn _{0.05} Co	162	201	227	178	215	245
Cu _{0.05} Co	180	225	257	206	248	287
Ni _{0.05} Co	170	213	245	199	243	290
Fe _{0.05} Co	169	210	241	184	219	255

Likewise, the catalytic reaction rates of all catalysts in the propane oxidation at 160 °C were calculated and are listed in Table 6. They followed the order, Co₃O₄ ≈ Mn_{0.05}Co > Fe_{0.05}Co ≈ Ni_{0.05}Co > Cu_{0.05}Co. In addition, from Arrhenius plots (Figure S3b), various E_a (67–79 kJ mol⁻¹) were obtained (Table 6). Compensation effect appeared again (Figure S4) [23,24], namely, the higher the value of E_a, the higher the value of lnA.

Table 6. Reaction rates (r) at 160 °C, apparent pre-exponential factors (A), apparent activation energies (E_a), and coefficient of determination (R²) for propane oxidation over various catalysts (reaction conditions: propane concentration = 1000 ppm, O₂ concentration = 21 vol.% and WHSV = 40,000 mL h⁻¹ g⁻¹).

Catalysts	r (10 ⁻⁸ mol gCo ⁻¹ s ⁻¹)	lnA	E _a (kJ mol ⁻¹)	R ²
Co ₃ O ₄	6.1	4.2 ± 0.2	76.2 ± 0.8	0.999
Mn _{0.05} Co	6.1	3.0 ± 0.3	72.0 ± 0.9	0.999
Cu _{0.05} Co	3.0	0.8 ± 0.1	66.8 ± 0.4	0.999
Ni _{0.05} Co	4.2	2.3 ± 0.2	70.9 ± 0.7	1.000
Fe _{0.05} Co	4.2	4.5 ± 0.2	78.6 ± 0.7	0.999

As in every oxidation process, water is inevitably present either as a part of the inlet stream or as a combustion product, which would alter reaction equilibrium and in turn cause deactivation, due to either the competitive adsorption between H₂O and reactant molecules or the formation of inert hydroxyls groups on the catalyst surface [26]. Therefore, the effect of presence of H₂O on the catalytic oxidation of propane was investigated. As shown in Figure 9, a decrease in propane conversion was observed for all studied catalysts when 4.4 vol.% of H₂O was present in the reactant gas. Their T₅₀ values were 9–30 °C higher than those obtained in the dry reaction condition. Among these catalysts, Fe_{0.05}Co presented the best water tolerance for propane oxidation since it maintained good activity to a certain extent. Ni_{0.05}Co was the most sensitive sample to H₂O. On the other hand, Mn_{0.05}Co still showed desirable catalytic performance, with T₁₀ as low as 178 °C.

**Figure 9.** Variation of the propane conversion with the reaction temperature during the cooling run over the Co₃O₄ and M_{0.05}Co catalysts in the absence and presence of 4.4 vol.% water.

2.4. Discussion

By metal doping, smaller crystalline sizes and larger specific surface areas were obtained for the $Mn_{0.05}Co$ catalyst. XRD and Raman analysis demonstrated that other metal (Mn, Cu, Ni, or Fe) was inserted into the structure of Co_3O_4 . This was corroborated by lattice expansion and broadening of Raman bands. Furthermore, FTIR spectra revealed that there were some metal oxides (Mn, Fe) distributed on the surface of Co_3O_4 . H_2 -TPR results confirmed the strong interaction between M and Co in the $Mn_{0.05}Co$ catalyst, as the reduction behavior changed much after M-doping.

The effect of the metal doping on the catalytic performance of all the catalysts in the toluene and propane oxidation reactions was not always the same. A catalyst that was active for toluene oxidation may not be good for propane oxidation. That was the case, for example, for catalyst $Cu_{0.05}Co$. This may be due to the different nature of these two reactant molecules (type of C–C bonds and molecular sizes) and the different reaction mechanisms involved for these two reactions [27]. It is generally accepted that the total oxidation of toluene over Co-based catalysts proceeds through a Mars–van Krevelen mechanism: toluene first reacts with the mobile lattice oxygen species to produce CO_2 and H_2O accompanied by the reduction of Co^{3+} to Co^{2+} , meanwhile O_2 molecules in air replenish the reduced catalyst and complete the redox cycle $Co^{3+} \rightleftharpoons Co^{2+}$ [28,29]. The promoted catalytic performance of $Cu_{0.05}Co$ and $Ni_{0.05}Co$ for toluene oxidation could be attributed to the strong synergistic effect between cobalt and doped metal cations. Lattice oxygen could be much more easily abstracted by hydrogen from $Cu_{0.05}Co$ and $Ni_{0.05}Co$ than from Co_3O_4 , increasing the mobility of lattice oxygen and resulting in better oxidation ability. For propane oxidation, the amount of surface adsorbed oxygen is reported to be the determining factor [30,31]. Thus, metal doping may influence the chemical status of surface/chemisorbed oxygen in $M_{0.05}Co$, thus leading to a different catalytic behavior in propane oxidation.

Anyhow, benefitting from its big strain and large surface area, $Mn_{0.05}Co$ is the best catalyst prepared in this study. It is efficient for both toluene and propane oxidation reactions. Hopefully, it could be considered as a potential industrial catalyst for removing hydrocarbon pollutants by oxidation processes.

3. Experimental

3.1. Catalyst Preparation

Cobalt oxide and M-doped (Mn, Fe, Ni, and Cu) cobalt oxide catalysts were prepared by a coprecipitation method using sodium carbonate as the precipitant. All chemicals were obtained from Sigma-Aldrich and used as received. Twenty millimoles of $Co(NO_3)_2 \cdot 6H_2O$ and 1 mmol of second metal salt ($Mn(Ac)_2 \cdot 4H_2O$, $Cu(NO_3)_2 \cdot 3H_2O$, $Ni(NO_3)_2 \cdot 6H_2O$, or $Fe(NO_3)_3 \cdot 9H_2O$) were dissolved in 100 mL of distilled water. Twenty-two millimoles of Na_2CO_3 was dissolved in 100 mL of distilled water. The resulting Na_2CO_3 aqueous solution was added to the metal salts aqueous solution. After being stirred at room temperature for 1 h, the solid was separated and fully washed by centrifugation and redispersion. The obtained wet cake was dried at 80 °C overnight and then calcined in a muffle furnace at 200 °C for 1 h and at 500 °C for 1 h with a temperature ramp rate of 2 °C/min⁻¹. The final products were referred to as $M_{0.05}Co$, where M is the doped metal and 0.02 is the atomic ratio of M:Co.

3.2. Catalyst Characterization

The chemical composition of the samples was measured by ICP-OES (Horiba Jobin Yvon, Paris, France). Prior to the determination, the metal oxides were dissolved in a mixture of inorganic acids (H_2SO_4 and HNO_3).

FTIR spectra were recorded using a FT-IR C92712 spectrometer (PerkinElmer, Waltham, MA, USA) in attenuated total reflectance mode at an instrument resolution of 1 cm⁻¹ over a range of 400 to 4000 cm⁻¹.

Nitrogen adsorption–desorption isotherms were obtained using a TRISTAR II apparatus (Micromeritics, Norcross, GA, USA) at $-196\text{ }^{\circ}\text{C}$. Before analysis, each sample was pretreated at $300\text{ }^{\circ}\text{C}$ for 3 h under primary vacuum. The specific surface areas of the samples were determined by the standard Brunauer–Emmett–Teller (BET) procedure. The total pore volume and the pore size distribution were calculated using the BJH method.

Powder X-ray diffraction (XRD) patterns were recorded on a D5005 diffractometer (Bruker, Karlsruhe, Germany) equipped with a Cu $K\alpha$ radiation ($\lambda = 0.154184\text{ nm}$) and a graphite monochromator on the diffracted beam. Samples were scanned from $10^{\circ} < 2\theta < 80^{\circ}$ with a step size of 0.02° and a counting time of 2 s per step.

Raman spectra were recorded by a LabRam HR spectrometer (Horiba, Paris, France) using Ar^+ laser beam of 514 nm wavelength for an excitation.

Temperature-programmed reduction experiments in hydrogen (H_2 -TPR) were performed on a commercial Micromeritics AutoChem 2950 HP (Micromeritics, Norcross, GA, USA) unit with TCD detection. In each test, 0.05 g of sample was pretreated under 50 mL/min of Ar flow at $350\text{ }^{\circ}\text{C}$ for 0.5 h . After cooling down to $45\text{ }^{\circ}\text{C}$, reduction was performed under 50 mL/min of $5\text{ vol.}\%$ H_2/Ar from 45 to $800\text{ }^{\circ}\text{C}$ at a rate of $10\text{ }^{\circ}\text{C/min}$. A trap cooled with isopropyl alcohol/liquid nitrogen slurry ($-80\text{ }^{\circ}\text{C}$) was applied to remove water that could distort the TCD signal.

3.3. Catalytic Activity Tests

For each test, 150 mg of catalyst mixed with $\sim 600\text{ mg}$ of silicon carbide was packed inside a U-shaped reactor (220 mm in length and 4 mm in internal diameter) with a bed height of 6 mm .

For the toluene oxidation tests, the reactant gas mixture, composed of 1000 ppm toluene and synthetic air ($21\text{ vol.}\%$ $\text{O}_2 + 79\text{ vol.}\%$ N_2), with a total flow of 100 mL/min , was fed into the reactor before being heated from room temperature to $150\text{ }^{\circ}\text{C}$ ($5\text{ }^{\circ}\text{C/min}$) and held at this temperature for 0.5 h to stabilize the system. Then, a second temperature ramp of $2\text{ }^{\circ}\text{C/min}$ was run until $350\text{ }^{\circ}\text{C}$ and held at this temperature for 1 h . Next, the reactor was cooled down to $150\text{ }^{\circ}\text{C}$ ($2\text{ }^{\circ}\text{C/min}$). Three consecutive heating–cooling catalytic cycles were performed to evaluate the catalytic stability. The concentrations of CO and CO_2 were in situ recorded by a Rosemount Xtreme Gas Infrared Analyzer (Emerson Electric Co., St. Louis, MO, USA). The toluene conversion was calculated as follows,

$$X_{\text{C}_7\text{H}_8}(\%) = \frac{[\text{CO}_2]}{7[\text{C}_7\text{H}_8]} \times 100 \quad (1)$$

where $[\text{CO}_2]$ and $[\text{C}_7\text{H}_8]$ represent the outlet CO_2 concentration and the initial toluene concentration, respectively.

Regarding the propane oxidation, after 100 mL/min of the reactant gas mixture ($0.1\text{ vol.}\%$ propane + $21\text{ vol.}\%$ $\text{O}_2 + 79\text{ vol.}\%$ He) was introduced into the reactor at room temperature, the reactor was heated from room temperature to $100\text{ }^{\circ}\text{C}$ ($5\text{ }^{\circ}\text{C/min}$) and held at this temperature for 0.5 h to stabilize the system. Subsequently, the temperature was increased from $100\text{ }^{\circ}\text{C}$ to $350\text{ }^{\circ}\text{C}$ ($2\text{ }^{\circ}\text{C/min}$) and held at this temperature for 1 h . Next, the reactor was cooled down to $100\text{ }^{\circ}\text{C}$ ($2\text{ }^{\circ}\text{C/min}$). Gas effluents were analyzed by an online micro gas chromatograph (SRA % GC-R3000) coupled with a thermal conductivity detector. The propane conversion was calculated as follows,

$$X_{\text{C}_3\text{H}_8}(\%) = \frac{[\text{CO}_2]}{3[\text{C}_3\text{H}_8]} \times 100 \quad (2)$$

where $[\text{CO}_2]$ and $[\text{C}_3\text{H}_8]$ are the outlet CO_2 concentration and the initial propane concentration, respectively.

4. Conclusions

Cobalt oxides doped with Mn, Cu, Ni, or Fe were successfully synthesized via simple carbonate coprecipitation method. XRD and Raman analysis proved the formation of the cubic spinel phase

Co₃O₄ after the incorporation of dopants. The Mn_{0.05}Co sample exhibited the smallest crystalline size and biggest strain. The MnO_x and FeO_x phases could be detected on the surface of Mn_{0.05}Co and Fe_{0.05}Co by FTIR spectra. The H₂-TPR study demonstrated the strong interaction between doped metal and cobalt. Cu_{0.05}Co appeared to be the most reducible sample. The catalytic activities were investigated for the total oxidation of toluene and propane. Mn_{0.05}Co exhibited undoubtedly the highest catalytic activity in both reactions. However, the activity for toluene and propane oxidation for the other catalysts was different. Cu_{0.05}Co and Ni_{0.05}Co were more active in toluene oxidation than pure Co₃O₄, whereas the opposite occurred for propane oxidation. Although the doping of Fe lowered the activity of pure Co₃O₄ in both cases, it allowed for the acquisition of better water-resisting catalysts for propane oxidation. Different mechanisms and different rate-determining factors are supposed to explain this activity variation as a function of the molecules to be oxidized.

Supplementary Materials: The following are available online at <http://www.mdpi.com/2073-4344/10/8/865/s1>, Figure S1: Variation of the (a) toluene conversion (b) propane conversion with the reaction temperature during the heating run, Figure S2: Evolution of (a) CO concentration in toluene oxidation and (b) C₃H₆ concentration in propane oxidation during one heating-cooling catalytic cycle over the Co₃O₄ and M_{0.05}Co catalysts, Figure S3: Arrhenius plots for (a) toluene oxidation (b) propane oxidation over Co₃O₄ and M_{0.05}Co catalysts. (reaction conditions: toluene/propane concentration = 1000 ppm, O₂ concentration = 21 vol.% and WHSV = 40,000 mL h⁻¹ g⁻¹), Figure S4: Constable plot of apparent pre-exponential factors as a function of apparent activation energies for toluene and propane oxidation over Co₃O₄ and M_{0.05}Co catalysts, Figure S5: CO₂ evolution as a function of time on stream in air flow after 24-h stability test, Figure S6: Toluene conversion to CO₂ as a function of time on stream over Co₃O₄ catalyst at 230 °C.

Author Contributions: This study was done jointly by all authors. W.Z. prepared the catalysts, performed structural characterizations and catalytic oxidation tests, and wrote the manuscript. P.A. helped do nitrogen adsorption-desorption experiments. J.D.-R. made H₂-TPR experiments. C.D., J.L.V., and A.G.-F. coordinated the whole study, e.g., data interpretation, result discussion, and manuscript review and revision. All authors have read and agreed to the published version of the manuscript.

Funding: This research received no external funding.

Acknowledgments: This work was financially supported by the University Claude Bernard Lyon 1, the CNRS, and the Auvergne Rhone Alpes Region (project PAI 2019 LS 203067). We gratefully acknowledge the China Scholarship Council of P.R. China for Weidong ZHANG's grant, and Bomin FU for Raman spectra measurement.

Conflicts of Interest: The authors declare no conflict of interest.

References

1. Liu, Q.; Wang, L.-C.C.; Chen, M.; Cao, Y.; He, H.-Y.Y.; Fan, K.-N.N. Dry citrate-precursor synthesized nanocrystalline cobalt oxide as highly active catalyst for total oxidation of propane. *J. Catal.* **2009**, *263*, 104–113. [[CrossRef](#)]
2. Garcia, T.; Agouram, S.; Sánchez-Royo, J.F.; Murillo, R.; Mastral, A.M.; Aranda, A.; Vázquez, I.; Dejoz, A.; Solsona, B. Deep oxidation of volatile organic compounds using ordered cobalt oxides prepared by a nanocasting route. *Appl. Catal. A Gen.* **2010**, *386*, 16–27. [[CrossRef](#)]
3. Marin, R.P.; Kondrat, S.A.; Pinnell, R.K.; Davies, T.E.; Golunski, S.; Bartley, J.K.; Hutchings, G.J.; Taylor, S.H. Green preparation of transition metal oxide catalysts using supercritical CO₂ anti-solvent precipitation for the total oxidation of propane. *Appl. Catal. B Environ.* **2013**, *140*, 671–679. [[CrossRef](#)]
4. Salek, G.; Alphonse, P.; Dufour, P.; Guillemet-Fritsch, S.; Tenailleau, C. Low-temperature carbon monoxide and propane total oxidation by nanocrystalline cobalt oxides. *Appl. Catal. B Environ.* **2014**, *147*, 1–7. [[CrossRef](#)]
5. Tang, W.; Xiao, W.; Wang, S.; Ren, Z.; Ding, J.; Gao, P.-X. Boosting catalytic propane oxidation over PGM-free Co₃O₄ nanocrystal aggregates through chemical leaching: A comparative study with Pt and Pd based catalysts. *Appl. Catal. B Environ.* **2018**, *226*, 585–595. [[CrossRef](#)]
6. Li, G.; Zhang, C.; Wang, Z.; Huang, H.; Peng, H.; Li, X. Fabrication of mesoporous Co₃O₄ oxides by acid treatment and their catalytic performances for toluene oxidation. *Appl. Catal. A Gen.* **2018**, *550*, 67–76. [[CrossRef](#)]

7. Ren, Q.; Mo, S.; Peng, R.; Feng, Z.; Zhang, M.; Chen, L.; Fu, M.; Wu, J.; Ye, D. Controllable synthesis of 3D hierarchical Co_3O_4 nanocatalysts with various morphologies for the catalytic oxidation of toluene. *J. Mater. Chem. A* **2018**, *6*, 498–509. [[CrossRef](#)]
8. Wang, K.; Liu, B.; Cao, Y.; Li, Y.; Jia, D. V-modified Co_3O_4 nanorods with superior catalytic activity and thermostability for CO oxidation. *CrystEngComm* **2018**. [[CrossRef](#)]
9. Zhou, M.; Cai, L.; Bajdich, M.; García-Melchor, M.; Li, H.; He, J.; Wilcox, J.; Wu, W.; Vojvodic, A.; Zheng, X. Enhancing Catalytic CO Oxidation over Co_3O_4 Nanowires by Substituting Co^{2+} with Cu^{2+} . *ACS Catal.* **2015**, *5*, 4485–4491. [[CrossRef](#)]
10. Bae, J.; Shin, D.; Jeong, H.; Kim, B.-S.; Han, J.W.; Lee, H. Highly Water-Resistant La-Doped Co_3O_4 Catalyst for CO Oxidation. *ACS Catal.* **2019**, *9*, 10093–10100. [[CrossRef](#)]
11. Ren, Z.; Wu, Z.; Song, W.; Xiao, W.; Guo, Y.; Ding, J.; Suib, S.L.; Gao, P.-X. Low temperature propane oxidation over Co_3O_4 based nano-array catalysts: Ni dopant effect, reaction mechanism and structural stability. *Appl. Catal. B Environ.* **2016**, *180*, 150–160. [[CrossRef](#)]
12. Cai, T.; Huang, H.; Deng, W.; Dai, Q.; Liu, W.; Wang, X. Catalytic combustion of 1,2-dichlorobenzene at low temperature over Mn-modified Co_3O_4 catalysts. *Appl. Catal. B Environ.* **2015**, *166*, 393–405. [[CrossRef](#)]
13. Lou, Y.; Ma, J.; Cao, X.; Wang, L.; Dai, Q.; Zhao, Z.; Cai, Y.; Zhan, W.; Guo, Y.Y.; Hu, P.; et al. Promoting effects of In_2O_3 on Co_3O_4 for CO oxidation: Tuning O_2 activation and CO adsorption strength simultaneously. *ACS Catal.* **2014**, *4*, 4143–4152. [[CrossRef](#)]
14. Baidya, T.; Murayama, T.; Bera, P.; Safonova, O.V.; Steiger, P.; Katiyar, N.K.; Biswas, K.; Haruta, M. Low-temperature CO oxidation over combustion made Fe- and Cr-Doped Co_3O_4 catalysts: Role of dopant's nature toward achieving superior catalytic activity and stability. *J. Phys. Chem. C* **2017**, *121*, 15256–15265. [[CrossRef](#)]
15. Gonzalez-Prior, J.; Gutierrez-Ortiz, J.I.; Lopez-Fonseca, R.; Busca, G.; Finocchio, E.; de Rivas, B. Oxidation of chlorinated alkanes over Co_3O_4 /SBA-15 catalysts. Structural characterization and reaction mechanism. *Catal. Sci. Technol.* **2016**, *6*, 5618–5630. [[CrossRef](#)]
16. Yang, R.; Wang, Z.; Dai, L.; Chen, L. Synthesis and characterization of single-crystalline nanorods of α - MnO_2 and γ - MnOOH . *Mater. Chem. Phys.* **2005**, *93*, 149–153. [[CrossRef](#)]
17. Baldi, M.; Escribano, V.S.; Amores, J.M.G.; Milella, F.; Busca, G. Characterization of manganese and iron oxides as combustion catalysts for propane and propene. *Appl. Catal. B Environ.* **1998**, *17*, 175–182. [[CrossRef](#)]
18. Wang, Y.; Zhu, J.; Yang, X.; Lu, L.; Wang, X. Preparation of NiO nanoparticles and their catalytic activity in the thermal decomposition of ammonium perchlorate. *Thermochim. Acta* **2005**, *437*, 106–109. [[CrossRef](#)]
19. Liu, X.; Li, Z.; Zhang, Q.; Li, F.; Kong, T. CuO nanowires prepared via a facile solution route and their photocatalytic property. *Mater. Lett.* **2012**, *72*, 49–52. [[CrossRef](#)]
20. González-Prior, J.; López-Fonseca, R.; Gutiérrez-Ortiz, J.I.; de Rivas, B. Oxidation of 1,2-dichloroethane over nanocube-shaped Co_3O_4 catalysts. *Appl. Catal. B Environ.* **2016**, *199*, 384–393. [[CrossRef](#)]
21. Hu, H.; Cai, S.; Li, H.; Huang, L.; Shi, L.; Zhang, D. In situ DRIFTS investigation of the low-temperature reaction mechanism over Mn-Doped Co_3O_4 for the selective catalytic reduction of NO_x with NH_3 . *J. Phys. Chem. C* **2015**, *119*, 22924–22933. [[CrossRef](#)]
22. Chen, J.; Chen, X.; Xu, W.; Xu, Z.; Chen, J.; Jia, H.; Chen, J. Hydrolysis driving redox reaction to synthesize Mn-Fe binary oxides as highly active catalysts for the removal of toluene. *Chem. Eng. J.* **2017**, *330*, 281–293. [[CrossRef](#)]
23. Delimaris, D.; Ioannides, T. VOC oxidation over MnOx– CeO_2 catalysts prepared by a combustion method. *Appl. Catal. B Environ.* **2008**, *84*, 303–312. [[CrossRef](#)]
24. Hu, Z.; Wang, Z.; Guo, Y.Y.; Wang, L.; Guo, Y.Y.; Zhang, J.; Zhan, W. Total oxidation of propane over a Ru/ CeO_2 catalyst at low temperature. *Environ. Sci. Technol.* **2018**, *52*, 9531–9541. [[CrossRef](#)]
25. Huang, H.; Zhang, C.; Wang, L.; Li, G.G.; Song, L.; Li, G.G.; Tang, S.; Li, X. Promotional effect of HZSM-5 on the catalytic oxidation of toluene over MnOx/HZSM-5 catalysts. *Catal. Sci. Technol.* **2016**, *6*, 4260–4270. [[CrossRef](#)]
26. Feng, Z.; Zhang, M.; Ren, Q.; Mo, S.; Peng, R.; Yan, D.; Fu, M.; Chen, L.; Wu, J.; Ye, D. Design of 3-dimensionally self-assembled CeO_2 hierarchical nanosphere as high efficiency catalysts for toluene oxidation. *Chem. Eng. J.* **2019**, *369*, 18–25. [[CrossRef](#)]
27. García, T.; Solsona, B.; Taylor, S.H. Naphthalene total oxidation over metal oxide catalysts. *Appl. Catal. B Environ.* **2006**, *66*, 92–99. [[CrossRef](#)]

28. Bai, G.; Dai, H.; Deng, J.; Liu, Y.; Wang, F.; Zhao, Z.; Qiu, W.; Au, C.T. Porous Co₃O₄ nanowires and nanorods: Highly active catalysts for the combustion of toluene. *Appl. Catal. A Gen.* **2013**, *450*, 42–49. [[CrossRef](#)]
29. Genty, E.; Brunet, J.; Poupin, C.; Ojala, S.; Siffert, S.; Cousin, R. Influence of CO addition on the toluene total oxidation over Co based mixed oxide catalysts. *Appl. Catal. B Environ.* **2019**, *247*, 163–172. [[CrossRef](#)]
30. Ye, Z.; Giraudon, J.M.; Nuns, N.; Simon, P.; de Geyter, N.; Morent, R.; Lamonier, J.F. Influence of the preparation method on the activity of copper-manganese oxides for toluene total oxidation. *Appl. Catal. B Environ.* **2018**, *223*, 154–166. [[CrossRef](#)]
31. Li, X.; Li, X.; Zeng, X.; Zhu, T. Correlation between the physicochemical properties and catalytic performances of micro/mesoporous CoCeO mixed oxides for propane combustion. *Appl. Catal. A Gen.* **2019**, *572*, 61–70. [[CrossRef](#)]



© 2020 by the authors. Licensee MDPI, Basel, Switzerland. This article is an open access article distributed under the terms and conditions of the Creative Commons Attribution (CC BY) license (<http://creativecommons.org/licenses/by/4.0/>).